Hybrid solar cells with prescribed nanoscale morphologies based on hyperbranched semiconductor nanocrystals

Ilan Gur,[1,3] Neil A. Fromer[1], Chih-Ping Chen[2,4] Antonios G. Kanaras[1,2,#], and A. Paul Alivisatos[*,1,2,3]

[1]Materials Science Division, Lawrence Berkeley National Laboratory, Berkeley, California 94720

[2]Department of Chemistry, University of California, Berkeley, California 94720

[3]Department of Materials Science and Engineering, University of California, Berkeley, CA 94720

[4]Material and Chemical Research Laboratories, Industrial Technology Research Institute, Hsinchu 30013, Taiwan

[#] Current address: Department of Chemistry, The University of Liverpool, Liverpool, UK, L697ZD

[*] Correspondence should be addressed to A.P.A.

In recent years, the search to develop large-area solar cells at low cost has led to research on photovoltaic (PV) systems based on nanocomposites containing conjugated polymers. These composite films can be synthesized and processed at lower costs and with greater versatility than the solid state inorganic semiconductors that comprise today's solar cells. However, the best nanocomposite solar cells are based on a complex architecture, consisting of a fine blend of interpenetrating and percolating donor and acceptor materials. Cell performance is strongly dependent on blend morphology, and solution-based fabrication techniques

often result in uncontrolled and irreproducible blends, whose composite morphologies are difficult to characterize accurately. Here we incorporate 3-dimensional hyper-branched colloidal semiconductor nanocrystals in solution-processed hybrid organic-inorganic solar cells, yielding reproducible and controlled nanoscale morphology.

Early research in organic photovoltaic systems clearly demonstrated that excitons in conjugated polymers are best harvested via charge separation across a type II donor-acceptor (D-A) heterojunction with another material[1]. A variety of species - most notably small organic molecules[2], other polymers[3,4], C_{60}[5,6], and inorganic semiconductor nanocrystals[7-11] - have since been paired successfully with conjugated polymers in D-A nanocomposite solar cells. The short exciton diffusion lengths of most conjugated polymers require that these devices be based on a nanoscale composite active layer with a blended or bulk heterojunction[3,4]. The morphology of this nanocomposite layer strongly dictates the cells' performance. Polymer domains must be limited in dimension to twice the exciton diffusion length, typically 5-20 nm[12,13], for efficient exciton separation. In addition, both the donor and acceptor phases must form high-quality percolation networks spanning the thickness of the device to ensure efficient carrier collection at the electrodes. Governed by such stringent morphology requirements, processing of nanocomposite D-A heterojunctions is extremely sensitive and has been the subject of much research[6,14-17].

Constraints on morphology are especially challenging in hybrid nanocrystal-polymer blends[18,19]. The most efficient hybrid blends are currently prepared by spin-casting a co-

solution of nanocrystals and polymer from a two-solvent system. This process is far from optimal, as dispersion in the solvent relies on metastable solubility of the blend components. The resulting spin-cast film consists of a disordered blend whose specific morphology may vary based on differences in nanocrystal synthesis conditions and cleaning procedures. In addition, small variations in the solvent composition can cause large-scale separation of either blend component, with detrimental effects on device performance. Use of nanorods and small, branched nanoparticles has enhanced the performance of polymer-nanocrystal solar cells in recent years[7,8,20,21], allowing for improved electron transport vis-à-vis quantum dots. However, electron extraction is still limited in these devices by hopping through a percolation network of particles[22]. Moreover, the creation of percolation networks in these cells remains highly sensitive to solubility in the blend solutions, and morphological defects and deficiencies are common. Attempts to prescribe the morphology of hybrid blends using ordered templates are promising, but these designs require more complex fabrication methods and have yet to produce significant results[23-25]. This work presents hybrid solar cells whose blend morphology is insensitive to solubility and processing variations, for it is controlled entirely by the 3-D structure of a hyperbranched nanocrystal phase. These cells combine the simple processing and easy fabrication of nanocrystal blend cells with the ordered morphology and transport network of template-based systems.

We recently reported a synthetic method for the creation of 3-D dendritic inorganic nanocrystals with controlled size and branching structure[26]. As illustrated in **Fig. 1**, these hyperbranched nanocrystals allow the creation of hybrid solar cells, whose architecture affords advantages over conventional approaches. The branching structure of the

nanocrystals controls the dispersion of the inorganic phase in the polymer matrix, thus ensuring a large, distributed surface area for charge separation. Moreover, each hyperbranched particle spans the entire device thickness, and thus contains a built-in percolation pathway for transport of electrons to the anode. With decreased sensitivity to variations in processing, a monolayer of such nanocrystals in a polymer matrix provides a bulk heterojunction with the dispersion and percolation required for charge separation and transport. **Fig. 1** presents transmission electron micrographs of typical hyperbranched nanocrystals of cadmium selenide (CdSe) and cadmium telluride (CdTe). In this study, hyperbranched CdSe crystals as shown in **Fig. 1d** were integrated into a matrix of poly(3-hexylthiophene) (P3HT) to produce the hybrid solar cells. The CdSe/P3HT donor-acceptor pair is well understood, and thus serves as a model system for this investigation.

In order to explore the advantages of hyperbranched particles and the importance of their pre-formed percolation networks, we present a comparison between nanorod-polymer solar cells and hyperbranched nanocrystal-polymer solar cells, in which the percent of inorganic component is the same. Transmission electron micrographs of these nanocomposite films are shown in **Fig. 2**, for six different concentrations of CdSe. The images elucidate several differences. With increased loading, nanorods incorporate into the polymer matrix in a disordered manner, barely occupying some regions while forming large aggregates in others. In contrast, the hyperbranched particles populate the polymer matrix more deterministically. Similar in dimension to the thickness of the film, they are added contiguously, gradually approaching a well-defined monolayer with increased loading. The predefined shape of the hyperbranched particles eliminates

disorder that would otherwise arise from the uncontrolled population of smaller, rod-shaped particles. Beyond these geometrical considerations, one must keep in mind the processing differences between the two types of blends. Like organic dendrimers, hyperbranched nanocrystals are more easily processed from fine suspensions without aggregating[27]. Composites based on these 3-D particles can therefore be spin-cast from a single solvent, and are thus not prone to the large-scale phase separation frequently encountered in nanorod blends, which must be spun from a 2-solvent solution. Moreover, processing from a single solvent eliminates the long-range thickness variations of the P3HT matrix. Finally, spin-casting the final blend from pure chloroform, a good solvent for P3HT, may allow for improved crystallization of polymer domains in the final film, when compared to films cast from a blend.

The differences in morphology and dispersion between rod and hyperbranched nanocrystal composites manifest themselves in the operation of solar cells based on these separate systems. Solar cells based on both sets of composites illustrated in **Fig. 2** were prepared to demonstrate the advantages afforded by hyperbranched particles. **Fig. 3** presents a summary of operating characteristics for these cells, measured under simulated one-sun AM1.5 global illumination. Cells based on nanorods behave as previously observed. The nominal open circuit voltage (V_{oc}) of a P3HT-only device is measured at low nanorod loading, and is preserved until a threshold representing the formation of CdSe percolation networks across the device is reached (**Fig. 3a**). At this point, the V_{oc} rises to approach that of the complete heterojunction. A similar trend is observed in the short circuit current (J_{sc}) (**Fig. 3b**). Almost no carriers can be extracted from the device

at low loading; only when percolation networks begin to form in the nanocrystal phase can charge be extracted from the film.

Cells based on hyperbranched particles exhibit characteristically different behavior. With incorporation of only a small number of nanocrystals, the V_{oc} immediately rises to its full value of approximately 0.6 V, and remains constant with increased loading. That the device behaves like a complete heterojunction with so few particles is easily understood; each hyperbranched particle contains a pre-formed percolation path and can thus fully contribute to photovoltaic conversion. The absence of a threshold loading density is also evident in the J_{sc} of hyperbranched cells, as well as in the final power conversion efficiency (η) (**Fig. 3d**). In contrast with nanorod devices, cells based on hyperbranched particles show an immediate, near-linear rise in both J_{sc} and η with increased loading of CdSe, consistent with the idea that a single incorporated hyperbranched particle can contribute independently to the cell's output by virtue of its morphology.

In order to validate this model and ensure that the disparate device behavior illustrated in **Fig. 3** does in fact stem from a fundamental difference in percolation behavior of rod and hyperbranched nanocrystals, we performed a spectral analysis of the current output in these cells. **Fig. 4** presents photocurrent spectra from the rod (**Fig. 4a**) and hyperbranched particle (**Fig. 4b**) devices discussed above. The spectral response of pure P3HT, included for reference, is consistent with a measured absorption edge of 660 nm, beyond which the polymer is transparent to incident radiation. Any response from blend devices at wavelengths greater than 660 nm must therefore be the direct result of absorption events in the nanocrystalline phase. Thus, the relative current contribution

from this low-energy portion of a given spectrum directly reflects the degree to which carriers created in the CdSe are extracted from the device. Accordingly, we define a shape parameter, S, to be the integrated current from 660nm-750nm divided by the fully integrated photocurrent of the cell. Simply put, S is a measure of the cell's ability to extract charges created in the nanocrystals. **Fig. 4c** plots S as a function of CdSe loading for both nanorod and hyperbranched particle cells. The result is clear: a threshold concentration of CdSe is required to allow for the extraction of charges from nanorod CdSe. In contrast, hyperbranched CdSe particles can independently contribute to current generation, even at low concentrations, due to their intrinsically percolated structure.

A simple model of the hyperbranched nanocrystal solar cell emerges from the analysis above. Each hyperbranched particle embedded within the P3HT matrix represents a very small (roughly 150nm x 150nm x 150nm), yet fully functional hybrid solar cell. These independent single-particle cells are then effectively connected in parallel to create the full device. Data from hyperbranched particle cells support this picture of a simple parallel circuit: voltage remains constant with the addition of hyperbranched particles to the matrix, while the current is additive.

Based on this model, a well-defined, closed-packed monolayer of hyperbranched nanocrystals should yield the highest performance. This is indeed what the experiment shows. Increased CdSe loading in hyperbranched particle cells initially yields a nearly linear enhancement of power conversion efficiency, but this improvement saturates at high loading concentrations (**Fig. 3d**). Juxtaposed with the TEM images in **Fig. 2**, the device data show that cell performance levels off approximately when the hyperbranched

particles form a complete monolayer within the P3HT matrix. Thus, the optimization of hyperbranched particle cells proves simple, well defined, clearly characterized, and easily attained.

Though more easily fabricated, hyperbranched nanocrystal devices outperformed those made from nanorods in every parameter across all measured loading concentrations. Better performing nanorod cells have been reported, but achieving high performance is contingent upon hitting a 'sweet spot' in blend morphology, a difficult task given the system's sensitive dependence to processing conditions. In contrast, the composite architecture of hyperbranched particle cells affords a decreased sensitivity to small variations in loading concentration and processing. This is evident in a comparison of fill factor (FF) parameter between the two classes of devices. FF values, which reflect diode ideality and overall cell quality, are not only higher but much more constant in hyperbranched particle cells than nanorod cells across the range of loading ratios (**Fig. 3c**).

The ability to prescribe dispersion and percolation characteristics of a composite device through choice of nanoparticle structure is perhaps the clearest advantage of hyperbranched nanocrystal solar cells over other hybrid architectures. Still, the efficiencies cited here suggest that the CdSe nanocrystals used in this study are far from optimal. The specific hyperbranched nanocrystals described here have yielded cells with one-sun AM1.5G efficiencies as high as 2.2%, achieved via optimization of the deposition solvents and the annealing conditions. **Fig. 5** presents current-voltage characteristics for the highest efficiency device to date, alongside a high-magnification

TEM image of the composite used to make the cell. Close examination of the blend micrograph reveals that nearly optimal 5nm - 20nm P3HT domains are created between adjacent particles as a result of their urchin-like branching structure. Unfortunately, there appears to be little room for polymer to fully penetrate the branches of the individual nanocrystals, which would allow significantly more opportunity for efficient charge generation and collection. This suboptimal dispersion poses a synthetic challenge to create more open branching networks in hyperbranched CdSe nanoparticles. Investigating the effects of specific variations in particle size and branching structure on cell performance will help reveal the full potential of this approach, which holds great promise to enable simple fabrication of low cost, high efficiency hybrid solar cells.

We have demonstrated a novel architecture for hybrid nanocrystal-polymer solar cells, in which the internal 3-D structure of dentritic inorganic nanocrystals controls nanoscale blending and morphology in the active PV layer. By addressing morphology directly in the nanoparticle design, rather than the solution processing, the resulting devices offer significant practical advantages in fabrication and processing as compared to previous hybrid organic-inorganic composite solar cells..

Acknowledgements

Supporting Information Available: Detailed information on materials and methods is available free of charge via the Internet at http://pubs.acs.org.

References

1.   Tang, C. W. 2-Layer Organic Photovoltaic Cell. *Applied Physics Letters* **48**, 183-185 (1986).
2.   Janssen, R. A. J. et al. Photoinduced Electron-Transfer Reactions in Mixed Films of Pi-Conjugated Polymers and a Homologous Series of Tetracyano-P-Quinodimethane Derivatives. *Journal of Chemical Physics* **103**, 8840-8845 (1995).
3.   Halls, J. J. M. et al. Efficient Photodiodes from Interpenetrating Polymer Networks. *Nature* **376**, 498-500 (1995).
4.   Yu, G. & Heeger, A. J. Charge separation and photovoltaic conversion in polymer composites with internal donor/acceptor heterojunctions. *Journal of Applied Physics* **78**, 4510-4515 (1995).
5.   Yu, G., Gao, J., Hummelen, J. C., Wudl, F. & Heeger, A. J. Polymer Photovoltaic Cells - Enhanced Efficiencies Via a Network of Internal Donor-Acceptor Heterojunctions. *Science* **270**, 1789-1791 (1995).
6.   Shaheen, S. E. et al. 2.5% efficient organic plastic solar cells. *Applied Physics Letters* **78**, 841-843 (2001).
7.   Huynh, W. U., Dittmer, J. J. & Alivisatos, A. P. Hybrid nanorod-polymer solar cells. *Science* **295**, 2425-2427 (2002).
8.   Sun, B. Q., Marx, E. & Greenham, N. C. Photovoltaic devices using blends of branched CdSe nanoparticles and conjugated polymers. *Nano Letters* **3**, 961-963 (2003).
9.   Arango, A. C., Carter, S. A. & Brock, P. J. Charge transfer in photovoltaics consisting of interpenetrating networks of conjugated polymer and TiO2 nanoparticles. *Applied Physics Letters* **74**, 1698-1700 (1999).
10.   Beek, W. J. E., Wienk, M. M., Kemerink, M., Yang, X. N. & Janssen, R. A. J. Hybrid zinc oxide conjugated polymer bulk heterojunction solar cells. *Journal of Physical Chemistry B* **109**, 9505-9516 (2005).
11.   Arici, E., Sariciftci, N. S. & Meissner, D. Hybrid solar cells based on nanoparticles of CuInS2 in organic matrices. *Advanced Functional Materials* **13**, 165-171 (2003).
12.   Halls, J. J. M., Pichler, K., Friend, R. H., Moratti, S. C. & Holmes, A. B. Exciton diffusion and dissociation in a poly(p-phenylenevinylene)/C[sub 60] heterojunction photovoltaic cell. *Applied Physics Letters* **68**, 3120-3122 (1996).
13.   Savenije, T. J., Warman, J. M. & Goossens, A. Visible light sensitisation of titanium dioxide using a phenylene vinylene polymer. *Chemical Physics Letters* **287**, 148-153 (1998).
14.   Ma, W. L., Yang, C. Y., Gong, X., Lee, K. & Heeger, A. J. Thermally stable, efficient polymer solar cells with nanoscale control of the interpenetrating network morphology. *Advanced Functional Materials* **15**, 1617-1622 (2005).
15.   Chirvase, D., Parisi, J., Hummelen, J. C. & Dyakonov, V. Influence of nanomorphology on the photovoltaic action of polymer-fullerene composites. *Nanotechnology* **15**, 1317-1323 (2004).

16. Hoppe, H. et al. Nanoscale morphology of conjugated polymer/fullerene-based bulk-heterojunction solar cells. *Advanced Functional Materials* **14**, 1005-1011 (2004).
17. Watkins, P. K., Walker, A. B. & Verschoor, G. L. B. Dynamical Monte Carlo modelling of organic solar cells: The dependence of internal quantum efficiency on morphology. *Nano Letters* **5**, 1814-1818 (2005).
18. Huynh, W. U., Dittmer, J. J., Libby, W. C., Whiting, G. L. & Alivisatos, A. P. Controlling the morphology of nanocrystal-polymer composites for solar cells. *Advanced Functional Materials* **13**, 73-79 (2003).
19. Liu, J. S., Tanaka, T., Sivula, K., Alivisatos, A. P. & Frechet, J. M. J. Employing end-functional polythiophene to control the morphology of nanocrystal-polymer composites in hybrid solar cells. *Journal of the American Chemical Society* **126**, 6550-6551 (2004).
20. Sun, B. Q., Snaith, H. J., Dhoot, A. S., Westenhoff, S. & Greenham, N. C. Vertically segregated hybrid blends for photovoltaic devices with improved efficiency. *Journal of Applied Physics* **97**, - (2005).
21. Huynh, W. U., Peng, X. G. & Alivisatos, A. P. CdSe nanocrystal rods/poly(3-hexylthiophene) composite photovoltaic devices. *Advanced Materials* **11**, 923-+ (1999).
22. Greenham, N. C., Peng, X. G. & Alivisatos, A. P. Charge separation and transport in conjugated-polymer/semiconductor-nanocrystal composites studied by photoluminescence quenching and photoconductivity. *Physical Review B* **54**, 17628-17637 (1996).
23. Coakley, K. M. & McGehee, M. D. Photovoltaic cells made from conjugated polymers infiltrated into mesoporous titania. *Applied Physics Letters* **83**, 3380-3382 (2003).
24. Coakley, K. M., Liu, Y. X., Goh, C. & McGehee, M. D. Ordered organic-inorganic bulk heterojunction photovoltaic cells. *Mrs Bulletin* **30**, 37-40 (2005).
25. Gur, I., Fromer, N. A. & Alivisatos, A. P. Controlled Assembly of Hybrid Bulk-Heterojunction Solar Cells by Sequential Deposition. *J. Phys. Chem. B* (2006).
26. Kanaras, A. G., Sonnichsen, C., Liu, H. T. & Alivisatos, A. P. Controlled synthesis of hyperbranched inorganic nanocrystals with rich three-dimensional structures. *Nano Letters* **5**, 2164-2167 (2005).
27. Frechet, J. M. J. Functional Polymers and Dendrimers - Reactivity, Molecular Architecture, and Interfacial Energy. *Science* **263**, 1710-1715 (1994).

Figure 1 Hyperbranched nanocrystal solar cells. Hyperbranched nanocrystal solar cells combine the ease of fabrication of spin-cast hybrid devices (**a**) with the controlled morphology of templated approaches (**b**). Defects such as islands and aggregates detrimental to the performance of conventional spin-cast hybrid cells are eliminated in hyperbranched particle composites, where blend morphology is dictated entirely by the 3-D structure of the hyperbranched nanocrystal (**c**). Moreover, the hyperbranched particles span the entire thickness of the active film, thereby enhancing electron transport and eliminating the need for strict control of particle dispersion within the matrix. In **d** and **e**, transmission electron micrographs show the 3-D structure of CdSe and CdTe hyperbranched nanocrystals, respectively. Scale bar, 100nm.

Figure 2 Composite morphologies. Transmission electron micrographs illustrate morphologies of hybrid blends employing hyperbranched nanocrystals (**a**) alongside those composed of nanorods (**b**) at a variety of loading densities. Loading percentages in all figures represent concentration of CdSe in spin-casting solution by volume. Scale bar, 500nm.

Figure 3 Hybrid solar cell characteristics. Device characteristics for cells based on the blends shown in Fig. 2 elucidate fundamental differences between the operation of hyperbranched nanocrystal (solid circle, red) and nanorod (open circle, blue) solar cells. Data points, presenting the highest measured values from a set of 8 regions of each substrate, are representative of the defect-free device performance and reflect the generally observed trend.

Figure 4 Spectral analysis. Photocurrent spectra of hybrid cells based on hyperbranched-particles (**a**) and nanorods (**b**) are compared. Parameter S is derived from these plots to reflect contribution to the photocurrent exclusively as a result of CdSe absorption events. A plot of S vs. loading density for nanorod (open circle, blue) and hyperbranched nanocrystal (solid circle, red) solar cells elucidates the self-contained percolation structure of hyperbranched nanocrystals. $S = \dfrac{\int_{660nm}^{750nm} EQE(\lambda) \bullet d\lambda}{\int_{350nm}^{750nm} EQE(\lambda) \bullet d\lambda}$

Figure 5 Current-voltage characteristics and detailed morphology. Current-voltage characteristics for a hyperbranched nanocrystal cell with a one-sun AM1.5G efficiency of 2.18% (**a**) is presented alongside a TEM micrograph illustrating detailed morphology of this blend (**b**). Cell presented here are limited in performance by the tight branching in these prototype hyperbranched particles. Scale bar, 20nm.
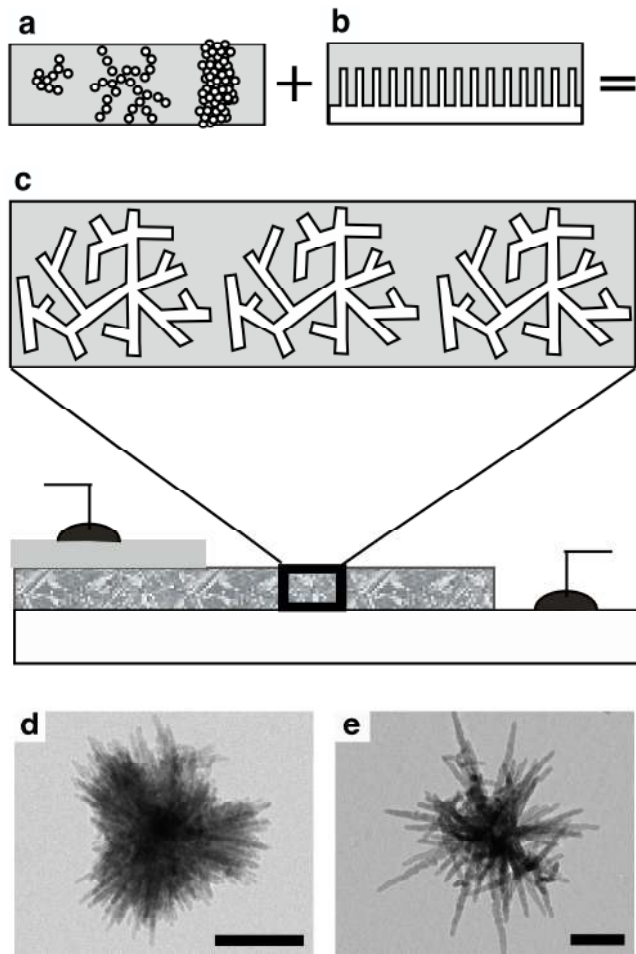
Figure 1

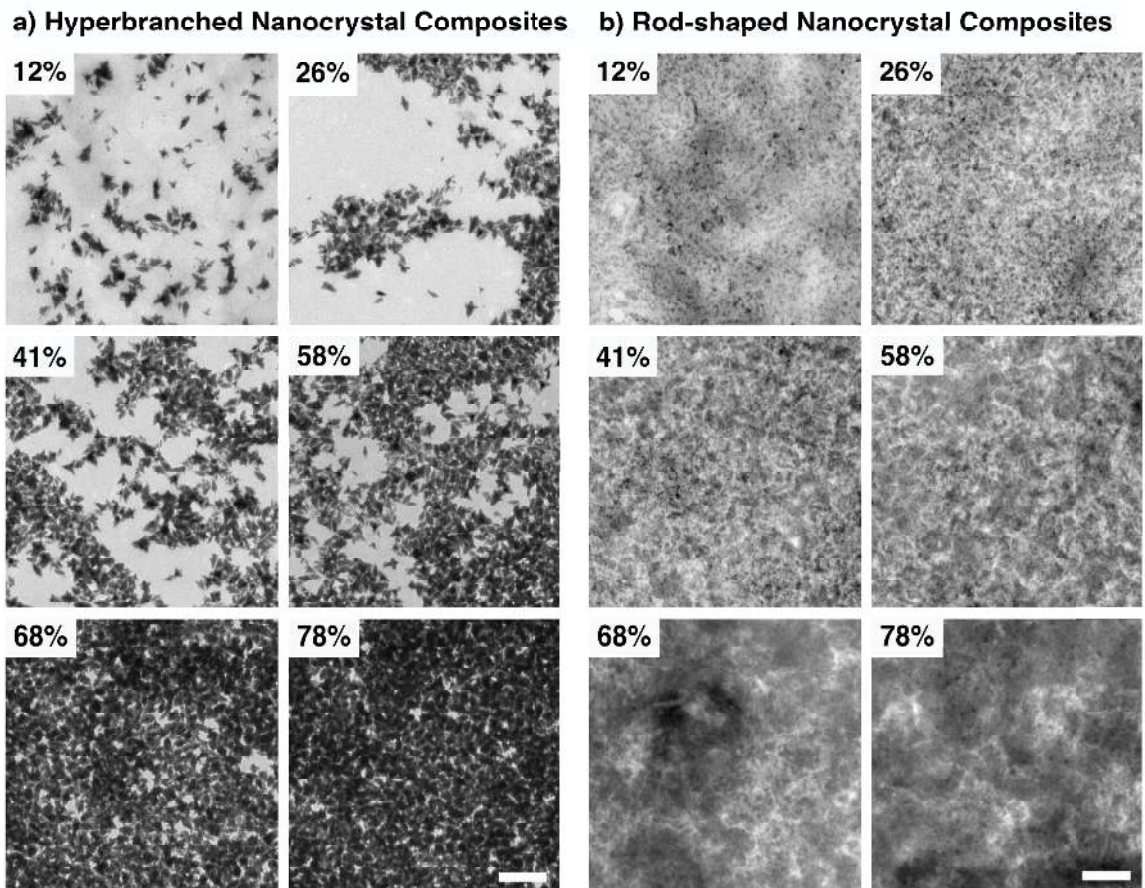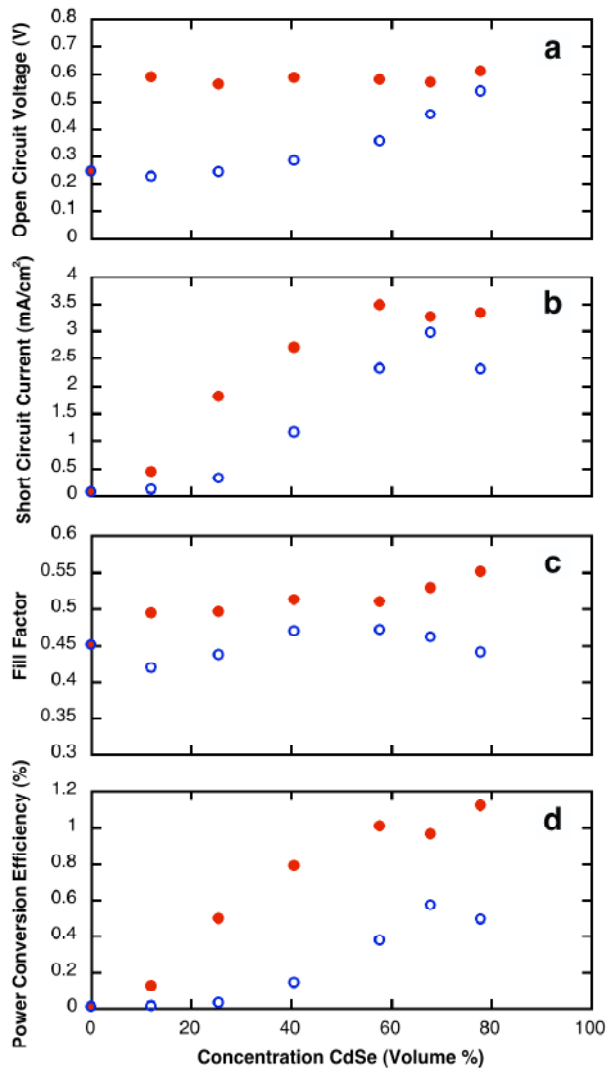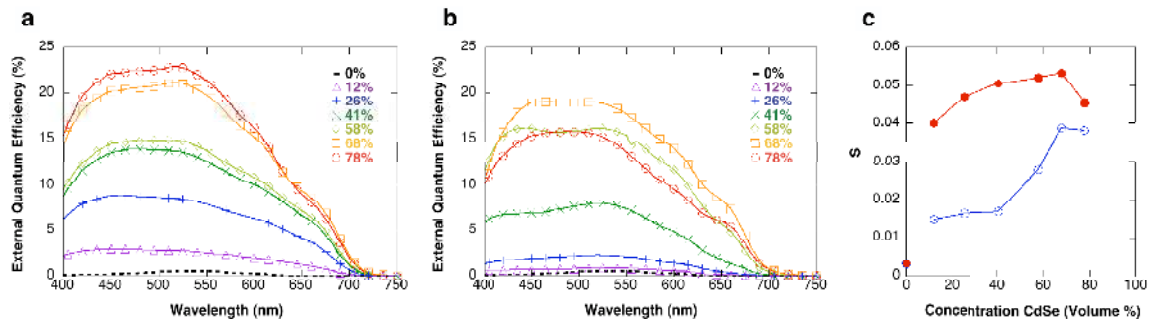**Figure 2**

Figure 3

Figure 4

Figure 5
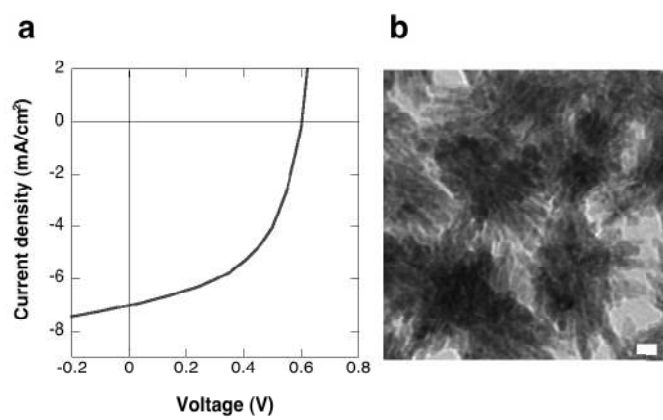
Table of Contents Figure